ACS OMEGA

Open Access

http://pubs.acs.org/journal/acsodf

Article

Experimental Study on the Erosion−Corrosion Characteristics of Desulfurization Slurry on Stainless Steel Pipe Materials

Gaofeng Fan, Jinming Zhang, Tianlin Yuan, Chang'an Wang,* Yujie Hou, Xinyue Gao, Jie Xu, and Defu Che

Cite This: *ACS Omega* 2024, 9, 7132−7142

Read Online

ACCESS | Metrics & More | Article Recommendations

ABSTRACT: The recovery of low-grade waste heat from power plants greatly benefits energy conservation and emission reduction during electricity generation, while the waste heat utilization directly from desulfurization slurry is a significantly promising method to deeply recover such low-grade energy and has been developed in practical application. However, the pipe materials are subjected to erosion and corrosion challenges due to the high level of solid compositions and the presence of harmful ions, such as Cl^{-1}, which requires further evaluation under the condition of slurry heat exchange. The present study aimed at an experimental study on the erosion−corrosion characteristics of desulfurization slurry on three types of stainless steel, including type 304, 316L, and 2205. Both mass loss and micromorphology features were analyzed with possible mechanisms elucidated. The erosion−corrosion rate is weak at low temperatures, while the increase in the slurry temperature clearly promotes its rate. The influence of the temperature on the corrosion resistance of 304 is much greater than that of 2205. With an increase in duration time, the weight loss rate of stainless steel in the desulfurization slurry declines, and the changing trend of metal mass slightly slows down. The present study offers a better understanding of the erosion−corrosion behaviors of three types of stainless steel under flow and heat transfer conditions of a desulfurization slurry.

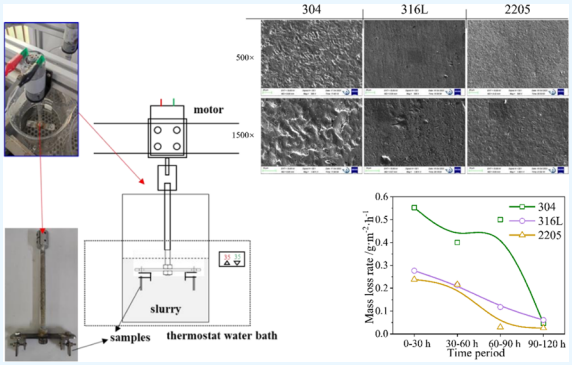

1. INTRODUCTION

The deep recovery of low-grade waste heat from flue gas can clearly improve the thermal efficiency of power plants, which benefits energy conservation and emission reduction during electricity generation.[1−4] Wet flue gas desulphurization has been extensively used in coal-fired power plants all over the world, which is mature, reliable, and applicable in industry with a high desulphurization efficiency.[5,6] After the desulphurization process, both flue gas and slurry contain abundant low-grade heat.[7,8] It is necessary to recover waste heat. The ordinary waste heat utilization technologies from flue gas are possibly confronted with some challenges such as complex systems, large investments, and increasing power consumption. The waste heat utilization directly from desulphurization slurry is another promising method to recover such low-grade energy, which has a large potential and has been developed in practical application.[9,10] The heat exchanger of the slurry can be directly used to heat network return water, heat condensate water, preheat air, and preliminarily dry fuel. This allows for the utilization of waste heat and further reduces expenses. In fact, the essence of recovering waste heat from desulfurization slurry is the deep recovery of flue gas waste heat as well.

Nevertheless, the high level of solid compositions within desulphurization slurry, such as ash particles, $CaCO_3$, $CaSO_4$, and other inert materials, can lead to erosion in the heating transfer system. In addition, the acidic property and the presence of F^{-1}, Cl^{-1}, and SO_4^{-2} can result in a corrosive attack on metal pipes, giving rise to the destruction of slurry pipes or/and heat exchanger of waste heat recovery.[11] Consequently, the effects of various influencing factors on the erosion and corrosion behaviors of pipe materials are of great importance for effectively controlling the erosion and corrosion performance of slurry heating transfer systems.

Stainless steel plays a vital role in many applications due to its excellent mechanical properties and corrosion resistance, which can be effectively employed in the flow and heat transfer of desulphurization slurry. A thin oxide film on the surface is mainly responsible for corrosion resistance, which is highly

Received: November 14, 2023
Revised: January 13, 2024
Accepted: January 16, 2024
Published: February 2, 2024

related to alloying elements, such as chromium (Cr), nickel (Ni), molybdenum (Mo), etc. The different structures of the metal matrix can be realized by adding alloying elements and applying specific heat treatments. The pearlite, bainite, martensite, and austenite are typical microscopic components in the metal matrix,[12] resulting in various types of stainless steel.

Many scholars have been devoted to the corrosion behaviors of various types of stainless steel. Krawczyk et al.[13] investigated the corrosion behaviors of 316L stainless steel in hydrochloric acid (HCl)-containing environments and found that the corrosion rate and type were mainly influenced by a rise in HCl concentration and electrolyte temperature under electrochemical control conditions, with corrosion type changing from pitting to mixed uniform and pitting mode and to uniform corrosion only. Dong et al.[14] probed the electrochemical behaviors of type 2205 stainless steel under conditions of various temperatures and NaCl contents, together with the mass loss tests after soaking for 24 h in solutions of $FeCl_3 \cdot 6H_2O$ and 1% HCl. The corrosion characteristics highly depended on temperature, and a temperature of 45 °C was the critical point. Zhou et al.[15] studied the corrosion feature of 2205 stainless steel using the electrochemical corrosion method. They concluded that corrosion occurred when the ferrite dissolved first to form pits. The local corrosion of 2205 mm stainless steel could be explained by the blocked battery model. The corrosive medium ions could move freely, oxygen could not pass through the rust layer blocking area, and a difference in oxygen concentration led to the formation of a battery to accelerate metal corrosion.

During the flow and heat transfer process of desulfurization slurry, except for corrosion, the erosion effect also exists and probably presents an interaction effect with corrosion and/or other electrochemical processes. Zhang et al.[16] investigated the wear and corrosion behaviors of type 1045 and 2205 stainless steel. They indicated that the protective passivation film could be damaged by wear, which accelerated corrosion in the wear area. Corrosion and wear had a synergistic effect. Chen et al.[17] studied the tribocorrosion of 316 in seawater and their results showed that the corrosion current density during erosion was much higher than that during static corrosion, while the erosion amount in seawater was much higher. Consequently, corrosion and erosion promoted each other under certain circumstances.

The most severe corrosion occurs in the slurry circulating pump and flow parts of the desulphurization slurry system. Nevertheless, the heat transfer system should also be given attention. Tian et al.[18] built a circulating loop system to probe the effects of particle size and shape on cast iron with various Cr contents. The corrosion was intensified with the increase in pH and chloride concentration. The effects of particle size varied with the environmental conditions. Parker et al.[19] used electrochemical experiments to study the mass loss of 2205 stainless steel in chlorine-containing media and without-chlorine media and concluded that the mass loss in chlorine-containing media was increased by 23−36%, and the presence of chloride ions also aggravated the local corrosion caused by erosion. Renner et al.[20] conducted an electrochemical wear test in a 3.5% NaCl solution. There was pitting corrosion under mild wear conditions but unobvious material loss occurred. Stack et al.[21] studied the interaction between potential and slurry concentration, which affected erosion−corrosion using the electrochemical method. The erosion−corrosion interactions varied with the external conditions. Islam and Farhat[22] established an electrochemical test system to study the synergistic effect of stainless steel tribocorrosion and to analyze the interaction between erosion and corrosion through weight reduction and microscopic observation. Wear removed the passivation film from the surface and destroyed the cementite network, resulting in subsurface cracks and deformable hardening, which exacerbated the corrosion. Aiming et al.[23] studied wear and corrosion in the pump and found that uniform corrosion and wear occurred in areas below the critical speed value, resulting in slight quality loss. The region where the speed was higher than the critical value was the region of nonuniform tribocorrosion, and the mass loss increased sharply with a rise in speed.

Dastgheib et al.[24] conducted a feasibility test evaluation on flue gas desulfurization of lime sludge. The corrosion resistances of carbon steel and stainless steel under various conditions were tested, and the results indicated that the corrosion resistance of stainless steel in the limestone slurry was obviously better than that of carbon steel. With the increase of Cl^- content in the slurry, the corrosion weight loss rate is obviously accelerated. The study of Smith et al.[25] revealed that the influence of Cl^- on the corrosion rate was different in different concentration stages. The increase of Cl^- content from 0.05 to 3.5% could lead to a remarkable increase in the corrosion rate, while the influence of Cl^- on the corrosion rate was unobvious in 3.5−10%. The chloride in molten salt could affect the corrosion behavior of stainless steel and then affect the integrity of the base metal structure. With the increase of chloride content in molten salt, both corrosion rate constant of 304 and 316L increased, but the corrosion of 304 was more serious.[26]

One main problem of the low-grade waste heat utilization of desulfurized slurries is wear corrosion. In the process of erosion−corrosion, the corrosive substances in the liquid could corrode the metal, and the liquid with abrasive suspended particles could cause wear to the parts through which the liquid flows. Maher et al.[27] summarized the synergistic effect of corrosion and erosion. On the one hand, erosion accelerated corrosion due to the removal of the passivation layer. On the other hand, corrosion could facilitate erosion when electrochemical dissolution produced friable external layers, which could then be destroyed by erosion in subsequent processes. There are many complex synergies between erosion and corrosion. The study of Shahali et al.[28] demonstrated that the change of erosion−corrosion caused by corrosion was higher than that caused by erosion under various conditions. This result emphasizes that the corrosion−erosion synergy is mainly dependent on the effect of corrosion on erosion. Slurry erosion−corrosion mainly occurs in steel pipes, extruders, and pumps. Elemuren et al.[29] studied the influence of solid concentration and flow rate on erosion−corrosion and probed the relationship between erosion and corrosion. For 1018 steel elbows, the synergies between erosion and corrosion reached 56% at a flow rate of 2.5 $m \cdot s^{-1}$, and they decreased to 11% at a flow rate of 4.0 $m \cdot s^{-1}$. Elemuren et al.[30] also carried out similar erosion−corrosion experiments on 2205 stainless steel. The results showed that the mass loss of 2205 was mainly caused by mechanical erosion, and the plastic deformation caused by the repeated impact of particles carried in liquid on the material surfaces was the main reason for the material stripping. Plastic deformation contributes to martensitic transformation a few micrometers below the erosion surface. However, other

https://doi.org/10.1021/acsomega.3c09065
ACS Omega 2024, 9, 7132−7142

literature has shown that the ferrite phase in 2205 is relatively easy to dissolve under acidification conditions, resulting in a higher corrosion rate.[31] In some cases, for high Cr content stainless steel, slight mechanical wear can form a more stable passivation film, which can improve corrosion resistance.[32] For different steels, a higher Cr/C ratio can improve the erosion−corrosion resistance of the material.[33]

In addition to different materials, the operating parameters of waste heat utilization devices are also crucial for erosion−corrosion. Ahmed et al.[34] described the influences of normal load, sliding distance, slurry concentration, and other operating parameters. The corrosion rates of different materials varied with different experimental parameters and material properties. Li et al.[35] conducted wear and corrosion tests on 304 stainless steel to consider the contribution rate of different operating parameters when they acted simultaneously. The results showed that the contribution rate of temperature to the corrosion rate was the highest, and the combined contribution of temperature, pH, and speed was greater than that of a single factor. The hardness of martensite in stainless steel is high, which has a certain effect on alleviating erosion−corrosion. The increase in slurry concentration and particle size has an obvious influence on the material quality loss, and the material shedding is mainly due to the wear caused by ploughing, microcutting, and plastic deformation. An increase in flow rate can lead to more erosion−corrosion, which can worsen when the flow rate exceeds the critical flow rate.[36] At the same time, the erosion−corrosion behavior at low particle concentration is determined by the properties of particles, and there are different corrosion behaviors for SiO_2 and Al_2O_3.[3737] Chung et al.[38] conducted erosion−corrosion tests on duplex stainless steel at different flow rates. The results demonstrated that the corrosion resistance of duplex stainless steel was higher at a low speed but the corrosion resistance was relatively poor at a high flow rate. Increasing the carbon content and thinning the structure are conducive to improving the corrosion resistance.

The significance of the present study is to explore the corrosion resistance of different types of stainless steel in the process of waste heat utilization of a desulfurization slurry under various conditions. The erosion−corrosion behaviors of stainless steel in desulfurized slurry were studied by setting up a simulated corrosion test platform so as to provide help in the process of waste heat utilization of the desulfurized slurry. Corrosion can be minimized by selecting the appropriate steel and setting the appropriate working parameters.

Although many scholars have carried out corrosion tests on various types of stainless steel under different conditions, most of them accelerate corrosion by electrochemical means, which possibly deviated from actual erosion behavior. In this experiment, a corrosion system was established to explore the erosion behavior close to actual operation. At the same time, due to the complexity of erosion−corrosion systems in industry, many studies were based on specific test equipment or parameters that could only be targeted at specific application conditions. It is difficult to translate directly to other applications such as the utilization of desulfurization slurry waste heat in slurry pipelines. The comparison among types 304, 316L, and 2205 under conditions of desulfurization slurry heat transfer has seldom been investigated. The dependences of temperature and chloride on the erosion−corrosion performance of 316L and 2205 stainless steel have yet to be fully understood. Here, the experimental research on the erosion−corrosion characteristics of desulfurization slurry on three types of stainless steel, including 304, 316L, and 2205, was conducted. The effects of slurry scour velocity, slurry temperature, chloride content, and exposure duration were mainly evaluated and discussed. The present study can offer a better insight into the erosion−corrosion process of stainless steel during the heat recovery process of desulphurization slurry.

2. EXPERIMENTAL SECTION

2.1. Samples. Three types of stainless steel, including 304, 316L, and 2205, were selected as experimental samples, which have been extensively employed in practical industry. The main chemical compositions of the three types of stainless steel are shown in Table 1. The samples were processed to a size of

Table 1. Chemical Compositions of Three Types of Stainless Steel Materials

	element contents (%)					
samples	Fe	Cr	Mn	Ni	Mo	V
304	72.51	17.39	1.03	8.10		
316L	69.70	15.93	1.66	10.13	2.03	0.192
2205	67.36	21.84	1.55	6.03	3.21	

$10 \times 20 \times 3$ mm^3, with a diameter of 4 mm at the top to fix the sample during experiments. The sample surfaces were polished with an abrasive paper of various meshes in turn before each test. Sandpaper of 180, 300, 800, 1200, 2000, and 3000 meshes were used in turn, and the final sample surface was 3000 mesh. After replacing the finer sandpaper, it is necessary to switch the grinding direction and grind until the previous roughness sandpaper grinding marks are removed to verify that the current coarse and fine sandpaper is completely polished. Then, the samples were placed into deionized water to process ultrasonic cleaning for 5 min and ultrasonically cleaned in absolute ethyl alcohol for another 5 min. Finally, the processed samples were stored in a ziplock bag for the subsequent experiments. The source of the three kinds of stainless steel is Jiangsu Metal Products Co., Ltd.

2.2. Experimental Setup. An experimental system was designed and built to investigate the erosion−corrosion characteristics of a desulfurization slurry on stainless steels, as depicted in Figure 1. The thermostat water bath was used to maintain a preset constant temperature with an accuracy of 1 °C. A shelf was built above the thermostat water bath to place the rotation motors, which were placed exactly centering the beaker. A reducing gear motor with a nonpolar voltage regulating power supply was selected, which can adjust the rotation speed in the range of 0−960 rpm. The variation in rotation speed can simulate the eroding velocity of desulfurization slurry on the surfaces of stainless steel materials. In the present study, six beakers can be placed in the thermostat water bath at one time, while two hanging slices were fixed at one motor by a specially designed fixture. Figure 1 depicts the schematic diagram of the experimental system for the erosion−corrosion tests, illustrating both overall and detailed images. The entire corrosion test was carried out in a container filled with slurry, and the sample was not exposed to air. At the same time, the container containing the slurry was immersed in a water bath, which could maintain the temperature of the container and the slurry at 30 and 65 °C. The temperature of the water bath was controlled to ensure the temperature of the slurry so as to ensure that the erosion

https://doi.org/10.1021/acsomega.3c09065
ACS Omega 2024, 9, 7132−7142

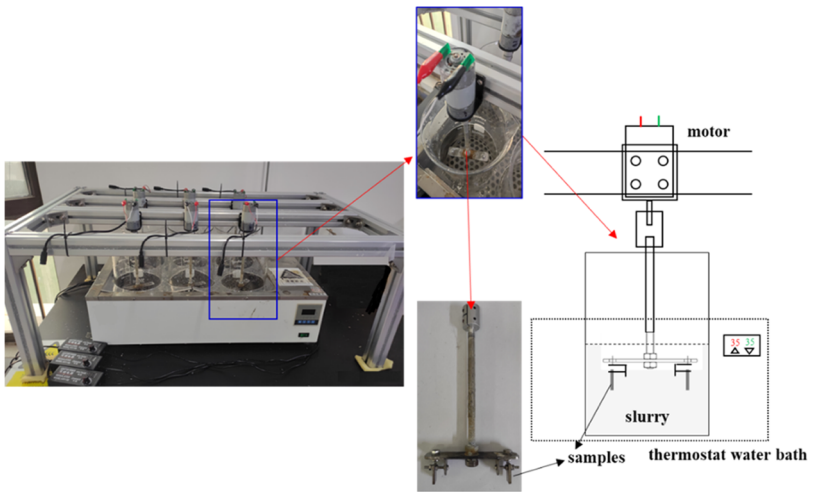

Figure 1. Schematic diagram of the experimental system for the erosion−corrosion tests.

behavior occurs at a constant setting temperature. Two beakers with identical parameters were set up for each working condition, and two samples were symmetrically arranged in each beaker. Corrosion weight loss test data were averaged from four samples to reduce experimental errors.

According to the practical operation of wet desulfurization, the solid content of desulfurization slurry accounts for about 20%, the Cl^- concentration is usually kept below 20,000 mg·L^{-1}, and the temperature of the slurry is controlled at about 65 °C during desulfurization. Here, the experimental parameters were set according to the practical operation, and some values were increased to enhance the corrosion effect when some specific parameters were investigated. Therefore, the influences of slurry scour velocity, temperature, Cl^- concentration, and exposure duration on the erosion−corrosion behaviors of stainless steel were studied in desulfurized slurry. When studying the effect of the rotation rate on corrosion behavior, the effects of the erosion rate on erosion characteristics were expected, the remaining conditions were set close to the weak acid condition of actual desulfurization slurry, and the pH of the final slurry during the experimental corrosion test was 7. When studying the influence of temperature and Cl^- concentration on corrosion, the influences of temperature on corrosion characteristics were obtained. In order to enhance corrosion, the pH value is increased in the process of sizing slurry to enhance the corrosion effect. Therefore, the pH of the sizing slurry was set at 2 to enhance the corrosion effect and highlight the influence of temperature and Cl^- concentration on the corrosion rate. The parameter setting of the corrosion test is shown in Table 2.

Generally, the temperature of desulfurization slurry is approximately 50 °C, with a content of 10−20% solid compositions, which are mainly $CaSO_4$ with a few inert compositions, $CaCO_3$, $MgCO_3$, CaF_2, fly ash, etc. The content of Cl^{-1} is about 20000 ppm with a pH of 5−6. In practical application, both erosion and corrosion consume quite a long time, which is extremely difficult and also unnecessary in lab-scale experiments. Hence, some parameters were selected to simulate and intensify the erosion and corrosion processes in lab-scale experiments. 100 g of quartz sand (SiO_2) and 150 g of calcium sulfate ($CaSO_4$) were added to 600 g of deionized water to simulate the desulfurization slurry, with a solid content of 29.4%. The inclusion of SiO_2 was used to accelerate the erosion process. Sodium chloride (NaCl) and hydrochloric acid (HCl) with a concentration of 1 mol·L^{-1} were both added to adjust the content of Cl^{-1} and pH value, which primarily contributes to the corrosion of slurry. During the experimental preparation of the slurry, a 1 mol·L^{-1} concentration of hydrochloric acid was used to adjust the pH value. The source of hydrochloric acid was Sinopharm Group Chemical Reagent Shaanxi Co., Ltd. All of the chemical reagents here were analytically pure, which benefits the exclusion of impurities. Here, the influences of eroding velocity, slurry temperature, chloride content, and duration time were mainly evaluated.

The rotation velocity of the hanging slice was adjusted by varying the DC supply voltage to the preset value, and then the slice was soaked into the simulated slurry by dropping off the motor support. The slurry level was continually monitored to avoid the obvious decline of the slurry from water evaporation. When the tests were finished, the sample slices were ultrasonically cleaned into deionized water for 5 min and then in absolute ethyl alcohol for another 5 min. After being dried, the sample slices were weighed and further analyzed with the aid of the scanning electron microscopy-energy dispersive spectroscopy (SEM-EDS) technique.

Table 2. Slurry Characteristics and Erosion−Corrosion Test Conditions

parameters	values
test duration	0−120 h
stirring motor speed	0, 300, 400, 500, 600, 700 rpm
slurry temperature	30 and 65 °C
solid insoluble content	29.4%
pH	2 and 7
Cl^- concentration	20,000 and 50,000 mg·L^{-1}

3. RESULTS AND DISCUSSION

3.1. Effects of Eroding Velocity. The eroding velocity of desulfurization slurry on the surfaces of stainless steel materials yields great impacts on the erosion−corrosion rate. Here, the rotation of the slice was constructed to simulate slurry eroding. The eroding velocity was adjusted by controlling the rotational velocity and position of the slice at the radial arm. In this section, the neutral slurry was used to emphasize the impacts of eroding velocity.

https://doi.org/10.1021/acsomega.3c09065
ACS Omega 2024, 9, 7132−7142

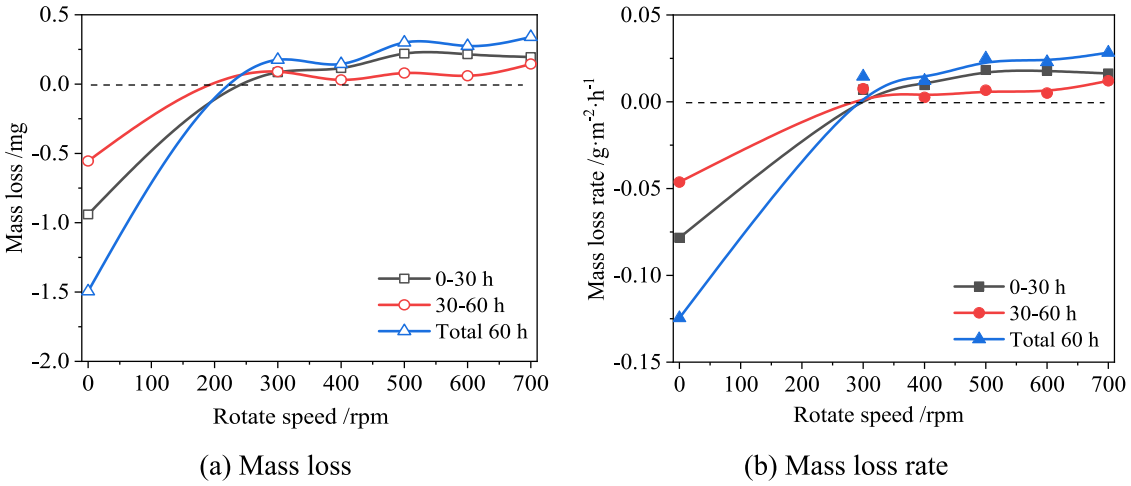

Figure 2. Effects of rotation speed on the mass loss characteristics of the type 304 sample: (a) Mass loss, (b) mass loss rate.

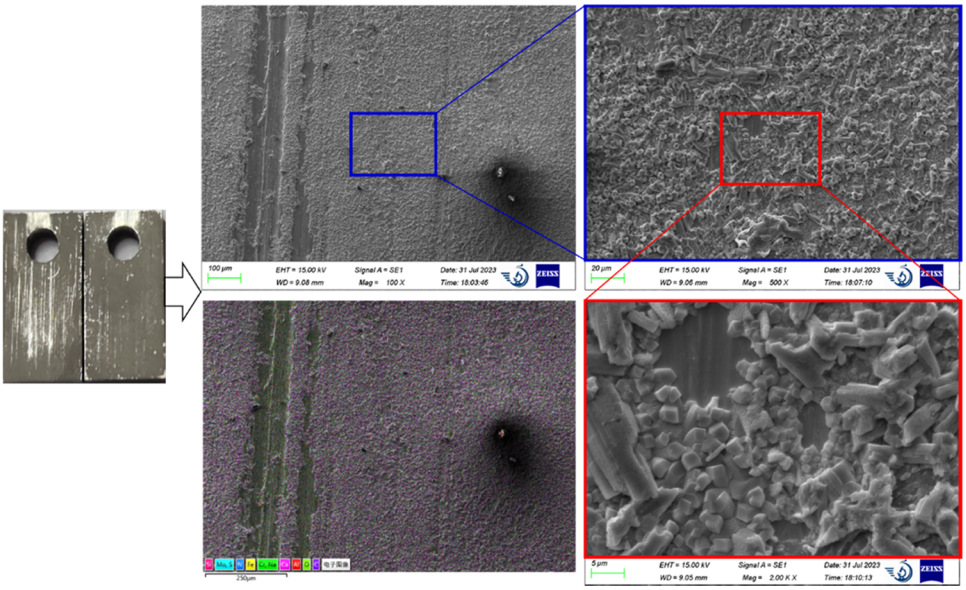

Figure 3. Micromorphology of the deposited sediment on surfaces of 304 stainless steel under conditions without eroding.

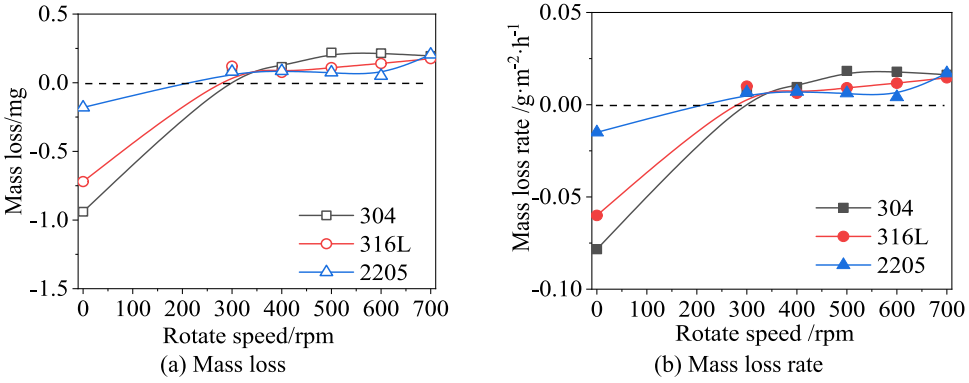

Figure 4. Comparison of weight reduction with the variation of rotation speed after 30 h among three stainless steels: (a) Mass loss, (b) mass loss rate.

Figure 2 depicts the effects of rotation speed on mass loss behaviors of the stainless steel 304 sample, with a Cl^{-1} content of 50,000 mg·L^{-1} and a slurry temperature of 65 °C. The 304 sample was first polished with abrasive paper and then underwent slurry erosion wear for 60 h. The positive value in Figure 2 implies the weight decline, while the negative value is the opposite. It can be seen from Figure 2a,b that with an increase in rotation speed, the weight reduction and mass loss rate are both limited, which exhibit only a small increase tendency. After the cleaning process, the sample surfaces are

https://doi.org/10.1021/acsomega.3c09065
ACS Omega 2024, 9, 7132−7142

bright, without clear erosion−corrosion. In addition, the mass loss in the former 30 h is higher than that in the latter 30 h. The erosion effect at the initial stage is predominant. Under the present experimental condition, the erosion−corrosion effect is considerably slight, possibly due to the limitation of duration time.

As depicted in Figure 2, the sample weight increases if the sample is only immersed in a slurry without rotation. An obvious deposit of sediment on the sample surface can be observed with the help of the scanning electron microscopy (SEM) technique, as illustrated in Figure 3. The energy dispersive spectrum (EDS) analysis confirms the possible presence of $CaSO_4$ crystals from slurry. Due to the existence of the eroding effect of slurry, it is difficult to form a $CaSO_4$ film on the sample surface.

The comparison of mass loss characteristics with rotation speed among three stainless steel materials is depicted in Figure 4, with a duration time of 30 h, a pH of 7, and a slurry temperature of 65 °C. The weight loss of the three samples presents similar variation with increasing rotation speed. When the rotation speed is zero, the weight increment of 304 is the maximum, followed by 316L, while that of 2205 presents the least mass variation. With the rotation of the hanging slice, both sediment deposition and cleanout have contributed to the weight variation of samples. However, at higher rotation speeds, the cleanout effect or eroding effect becomes the primary factor. As depicted in Figure 4a,b, the mass loss and mass loss rate of various samples at higher rotation speeds present the following sequence: 2205 < 316L < 304, which is quite similar to the condition of weight increase without rotation. Consequently, 2205 stainless steel generates the strongest erosive resistance to desulphurization slurry, not matter deposition or erosion.

Zhang et al.[16] captured the synergistic effect between corrosion and erosion, while the erosion mechanism differed between 1045 and 2205 stainless steel. The main erosion mechanism of type 2205 is abrasive and stratified wear. With the increase in erosion speed, both erosion loss and corrosion loss increase. With the increase in erosion velocity, the interaction between erosion and corrosion may decrease, and erosion gradually becomes dominant. The main causes of material weight loss at low erosion speed are fatigue shedding and erosion caused by plastic deformation, while the main cause of weight loss at high speed is erosion. The erosion and corrosion promote each other at low speed, while high eroding velocity possibly weakens the interaction due to the generation of a dense oxide layer.[39]

The hardness and chemical resistance of the material have important influences on the wear and corrosion behaviors. Low carbon steel due to low hardness and chemical corrosion resistance is the worst, which often shows a higher corrosion rate, while medium carbon steel, high carbon steel, and alloy steel are better than low carbon steel.[33] For 304, 316L, and 2205, 2205 has the highest strength, and 304 and 316L are similar but lower than 2205. In terms of hardness, 304 and 316L are lower than 2205 because 2205 contains the ferritic phase, which can strengthen the structural strength and improve the erosion resistance. At the same time, the scour velocity selected in the present experiment is relatively low. The highest scour velocity is about 0.5 $m \cdot s^{-1}$. It can be seen that the corrosion resistance of 2205 is the highest, followed by 316L, and 304 is the lowest when the erosion rate is relatively low, and the acidity of the slurry is very weak. The comparison between 316L and 304 shows that the physical properties, such as strength and hardness, cannot play a great role in corrosion resistance when the materials are mainly tested at a low flow rate. Their chemical composition and phase composition structure determine their ability to resist erosion−corrosion. The relevant research results also demonstrate that chemical corrosion is the main condition at a low flow rate, while the material removal rate caused by erosion at a high flow rate is quite high. Under the condition of corrosion-led erosion−corrosion, a certain hardness strength can significantly improve the erosion resistance.[40]

3.2. Effects of Slurry Temperature. The slurry temperature possibly slightly varies with operation conditions of the desulfurization process, while the temperature generally generates significant impacts on both erosion and corrosion behaviors of stainless steel materials. The effects of slurry temperature on weight reduction of three stainless steel samples are depicted in Figure 5, with a pH of 2, a rotation

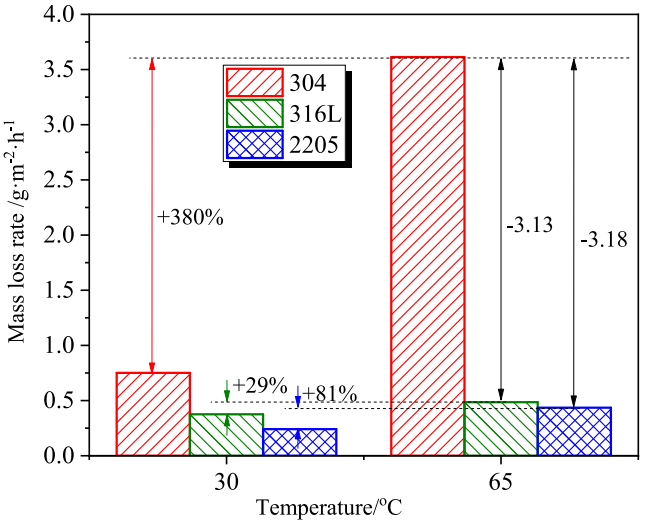

Figure 5. Effects of slurry temperature on weight reduction of three stainless steel samples.

speed of 500 rpm, a duration time of 30 h, and a chlorine content of 50,000 $mg \cdot L^{-1}$. All three samples were polished by 180, 320, 600, 1200, 2000, and 3000 meshes in turn. It can be observed from Figure 5 that the mass loss of stainless steel samples is relatively small at 30 °C, with the following sequence: 304 > 316L > 2205. When the temperature is increased to 65 °C, various degrees of mass loss rise are present, especially the mass loss rate of the 304 sample being raised by 380%. While the mass loss rates of 316L and 2205 samples only increase by 29 and 81%, respectively. As the slurry temperature is increased to 65 °C, the difference between 316L and 2205 is declined, whose mass losses are lower than that of the 304 sample by 3.13 and 3.18 $g \cdot m^{-2} \cdot h^{-1}$, respectively, as illustrated in Figure 5. The rise of slurry temperature strengthens the difference between the 304 sample and the other two materials but weakens the diversity between 316L and 2205 samples. It can be seen that the corrosion rates of the three kinds of stainless steel increase when the temperature rises, indicating that the temperature rise can lead to more intense corrosion behavior. When the temperature rises, the mass loss rate of 304 increases the most, while that of 316L and 2205 only increases slightly, which is

https://doi.org/10.1021/acsomega.3c09065
ACS Omega 2024, 9, 7132−7142

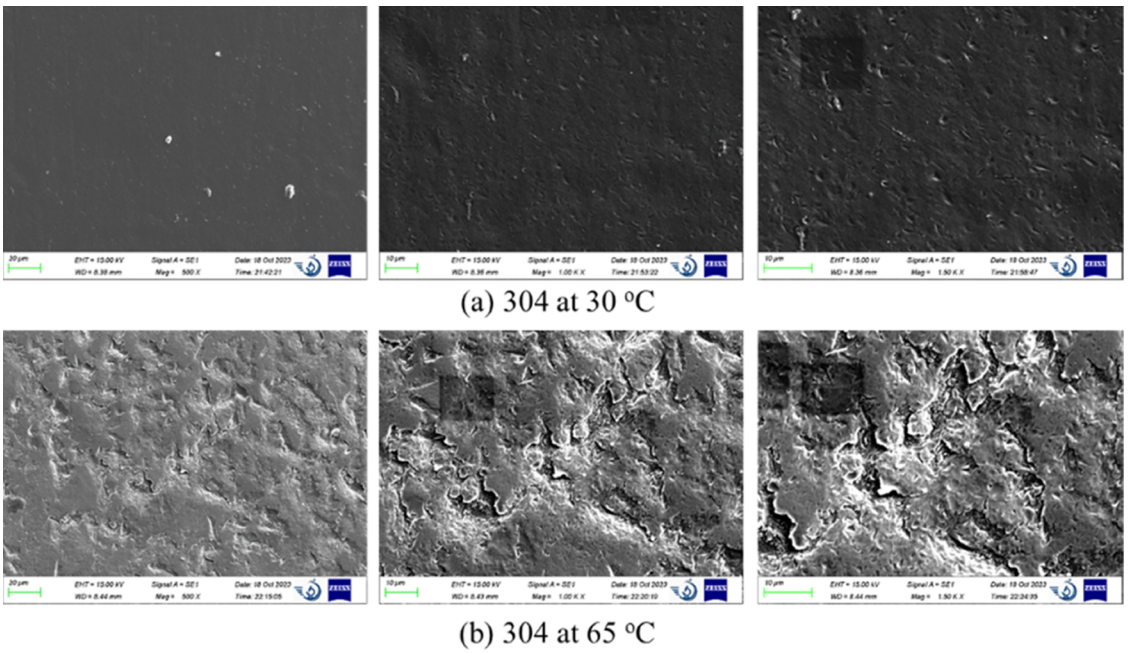

Figure 6. Comparison of the micromorphologies of the 304 sample between 30 and 65 °C conditions after the erosion−corrosion process.

similar to the result of 316L in Ahmed's study.[34] Sample 304 has a weak corrosion resistance at higher temperatures, while for the other two stainless steels, temperature has less of an effect on the corrosion rate.

The micromorphologies of the 304 sample after the erosion−corrosion process are compared in Figure 6. An obvious difference can be observed between conditions at 30 and 65 °C. The surface of the type 304 sample at 30 °C is relatively smooth with insignificant abrasion marks. However, the sample surface from the slurry at 65 °C shows intensive erosion−corrosion results, as depicted in Figure 6b. This finding is consistent with the mass loss results shown in Figure 5. Under the condition of 65 °C, the surface structure of the 304 sample is significantly destroyed. Small pits from the effects of the slurry can be observed, with a scaly texture left. The Cr element may dissolve out of the austenite phase, leading to the depletion of Cr at the crystal boundary. Cr has strong passivation and anticorrosion ability within stainless steel materials. The area with deficient Cr is easy to be corroded and then eroded by slurry.

For the comparison of the corrosion conditions at 30 and 65 °C, it can be seen from Figure 6 that the corrosion conditions at 30 °C are not serious, and only some corrosion pits appear. However, the corrosion conditions at 65 °C are relatively more obvious, and serious corrosion−erosion occurs. In addition, the surface materials are corroded and stripped, showing a scaly shape. Previous research has also shown that temperature could aggravate erosion−corrosion.[35]

The study of Smith et al.[25] showed that the influence of Cl^- on the corrosion rate was divided into two stages. The increase of Cl^- content in 0.05−3.5% leads to a significant increase in the corrosion rate, while the influence of Cl^- on the corrosion rate was unobvious in 3.5−10%. Dong et al.[14] probed the electrochemical behaviors of stainless steel type 2205 and observed the critical temperature of the mass loss rate. As the temperature exceeded 45 °C, the corrosion rate increased significantly. Krawczyk et al.[13] found that the corrosion rate of stainless steel 316L increased exponentially with temperature, since the hydrogen evolution overpotential decreased in HCl-containing environments, especially as the temperature was beyond 40 °C. The corrosion rate of the primary stainless steel is greatly temperature-dependent, but the critical point and quantitive temperature dependence vary with the environment and stainless steel type.

3.3. Effects of Chloride Content. Abundant chloride is probably present in the desulfurization slurry, and its content varies with operation conditions and coal properties as well. The high concentration of chloride ions could reduce the desulfurization efficiency and adversely affect the byproducts of wet desulfurization. Chloride is easy to induce pitting of stainless steel metal, resulting in metal failure and damage. In addition, the presence of chloride usually yields a corrosion effect on steel, while the anticorrosion ability of different materials to chloride differs greatly. Stainless steel type 304 is a single-phase austenitic steel without addition of plentiful alloying elements, so it cannot sufficiently inhibit the damage of chloride ions to the oxide film. For 316L, the addition of Mo element can inhibit the cracking of the oxide film and improve the passivation ability of stainless steel, which can better improve the chlorine corrosion resistance. In addition, 2205 also has good chlorine corrosion resistance due to the characteristics of duplex stainless steel and the addition of Mo and other alloying elements. Here, stainless steel types 316L and 2205 were selected to evaluate the effects of the chloride content. When studying the effect of Cl^- concentration on corrosion rate, the temperature was controlled at 65 °C, and the rotation speed was controlled at 500 rpm.

The effects of chloride content on the mass loss rate of 316L and 2205 samples are depicted in Figure 7, with a pH of 2, rotation speed of 500 rpm, a duration time of 30 h, and a slurry temperature of 65 °C. As the chloride concentration is increased from 20,000 to 50,000 $mg \cdot L^{-1}$, the mass loss rates of 316L and 2205 are raised by 32 and 93%, respectively. The difference of anticorrosion to chloride declined between 316L and 2205 samples with the rising chloride content in the slurry. A high level of chloride aggravates the erosion of steel materials

https://doi.org/10.1021/acsomega.3c09065
ACS Omega 2024, 9, 7132−7142

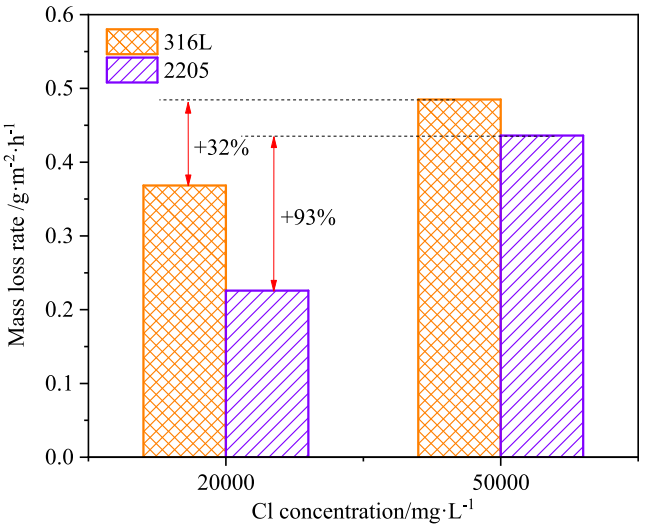

Figure 7. Effects of chloride content on the mass loss rate of stainless steel 316L and 2205 samples at 65 °C.

at high temperatures. Krawczyk et al.[13] found out that the corrosion type of 316L was a function of temperature and HCl concentration. Higher content of HCl implied a faster corrosion rate. The most significant change in the corrosion rate occurred with the temperature exceeding 40 °C, whereas the HCl concentration was likely to be the dominating parameter below 40 °C. The electrochemical behaviors of stainless steel type 2205 obtained by Dong et al.[14] indicated that NaCl concentration affected both corrosion rate and pitting structure, and the increased content of Cl^{-1} led to a more significant corrosion tendency of stainless steel 2205. The corrosion types varied from pitting corrosion, uniform corrosion, pitting, and uniform corrosion under conditions of various HCl contents and temperatures.[13] In addition, the electrochemical experiments conducted by Parker et al.[19] showed that the presence of chlorine-containing media increased the mass loss of stainless steel 2205 by 23−36% and also exacerbated the local corrosion caused by wear.

3.4. Effects of Duration Time. The time dependence of the erosion−corrosion behaviors also deserves special attention. The study of continuous mass variation over a long time can offer further information. Figure 8 shows the variation of average mass loss rate in different periods, with a

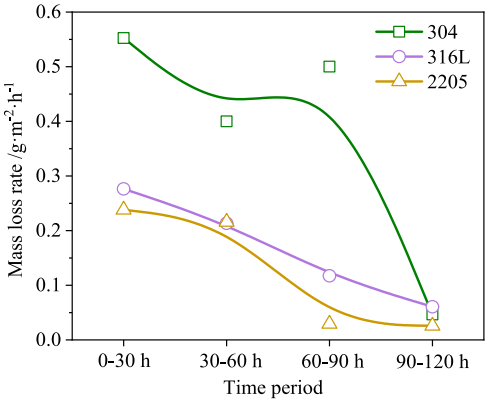

Figure 8. Variation of the average mass loss rate in various periods at 500 rpm.

pH of 2, a rotation speed of 500 rpm, a chloride concentration of 50,000 $mg·L^{-1}$, and a slurry temperature of 65 °C. The erosion and corrosion progress with the time of samples in slurry is prolonged, while the corrosion rate varies in various periods. With the duration prolonged, the mass loss rates of the three stainless steel samples declined. The formation of corrosion products and/or passive film possibly slows the further destruction of the parent metal. The material of the 2205 sample exhibits effective anticorrosion performance, which is highly related to its duplex ferritic-austenitic stainless characteristics. When the effect of time on the corrosion rate was studied, the temperature was controlled at 65 °C and the rotation speed was controlled at 500 rpm.

The comparison of micromorphologies of three stainless steel samples after erosion−-corrosion experiments for 120 h is depicted in Figure 9. The destruction phenomenon of the 304 sample surface is quite serious, with the presence of pits and a flaky texture. The EDS analysis indicates that the manganese (Mn) element enriches at the raised part of a flaky texture. It is reasonable to believe that the addition of Mn increases the hardness and abrasive resistance, which benefits the anti-corrosion performance in slurry. The erosion−corrosion issue of the 316L sample is slightly weaker than that of the 304 sample, with only a small hole being observed on surfaces. In addition, the appearance of the 2205 sample is similar to that of 316L, with only a slight corrosion mark present but without any large pieces of metal falling off. The duplex stainless steel, type 2205, for example, usually has the characteristics of high corrosion resistance in corrosive environments containing chloride ions, good resistance to corrosion, good mechanical strength, wear resistance, and good weldability.[41,42] The micromorphology comparison observation largely agrees with the mass loss results in Figure 8. In this experiment, the linear velocity of the sample surface is about 0.4 $m·s^{-1}$, and the flow rate is relatively small. In the case of a low flow rate, the erosion is mainly dominated by chemical corrosion. Therefore, in the early stage of the reaction, the corrosion rates of 2205 and 316L with better chemical corrosion resistance are lower, while 304 has a higher corrosion rate. At the same time, the damage ability of the passivation film on the surface of the material is limited in the state of a low flow rate. Hence, when the corrosion time gradually increases, the formation of a stable passivation film on the surface can effectively reduce the corrosion rate. Therefore, the corrosion efficiency of the three kinds of stainless steel gradually decreases, and the corrosion rate is only very small at 120 h.

In terms of corrosion mechanism, it is mainly divided into uniform corrosion, intergranular corrosion, electrochemical corrosion, and pitting corrosion. The corrosion in this study mainly corresponds to uniform corrosion and intergranular corrosion. In terms of the erosion mechanism, there are two erosion mechanisms. The first mechanism refers to the oblique impact of eroded particles with sufficient energy to break the surfaces of materials. The second mechanism occurs when the slurry is normally scoured, causing cracks or plastic deformation. In addition, the erosion mechanisms of ductile and brittle materials also differ from each other. Ductile materials are removed from the surface under the sideling impact, and a pit is formed under a positive impact. For brittle materials, both oblique impact and positive impact can form a large number of cracks on the surface of the target material.[27] For the conditions tested in the present study, there is an unobvious crack, which is related to the selected material and

https://doi.org/10.1021/acsomega.3c09065
ACS Omega 2024, 9, 7132−7142

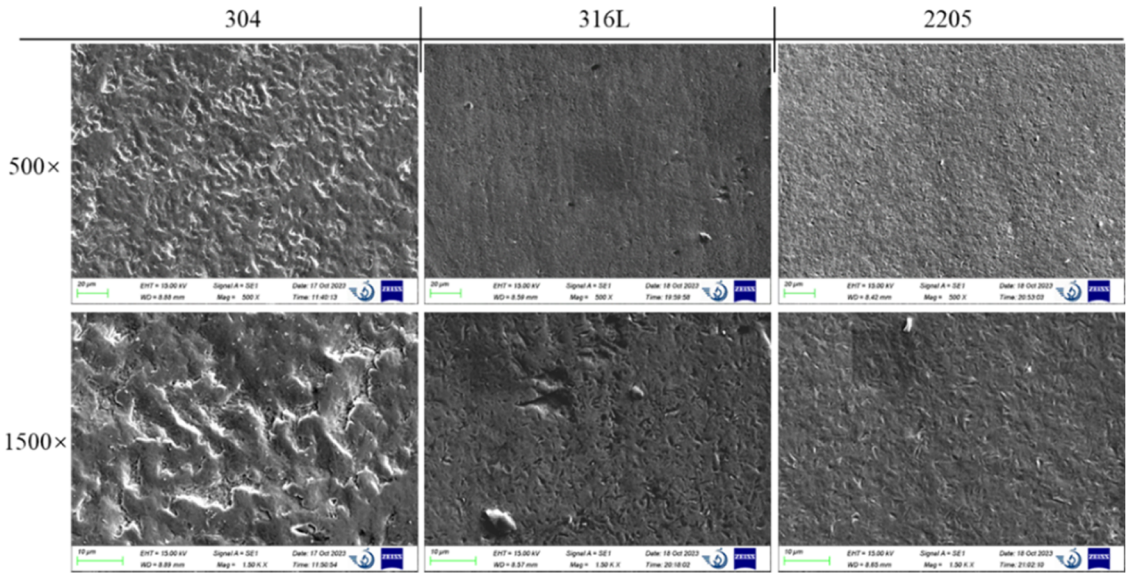

Figure 9. Micromorphologies of three stainless steel materials after erosion−corrosion tests of 120 h.

the impact angle, and the main erosion mechanism is cutting. When erosion and corrosion occur at the same time, the passivation layer is removed due to erosion, which accelerates the corrosion. On the other hand, corrosion can accelerate erosion when electrochemical dissolution produces a brittle surface layer, which can then be removed by erosion, and there is a complex synergistic relationship between erosion and corrosion. It can be seen that the selected three kinds of stainless steel have obvious corrosion traces, of which a 304 scaly surface indicates more serious erosion and its low chemical resistance is the cause of serious erosion. There are three possible synergistic effects of erosion−corrosion. One synergistic mechanism is to make the steel surface rough by generating fiber textures on the steel surface, which increases the local electric field and leads to a high corrosion rate. There are also scholars who say that the impact particles deform the surface, making it unstable. The destruction of the passive layer, resulting in exposure to an unprotected surface, tends to cause a higher rate of corrosion of the material.

Erosion−corrosion is a type of damage associated with the synergistic effects of mechanical, chemical, or electrochemical processes. Erosion−corrosion wear is a complex physical and chemical process. The formation of the passivation film can be conducive to preventing corrosion, but mechanical wear leads to the destruction or removal of the passivation film. A synergistic effect between corrosion and wear can be generated in the process of friction corrosion.[43] The interaction between erosion and corrosion is generally a difficult problem to solve. The plastic deformation caused by wear has a high dislocation density and corrosion activity and acts as an anode in the electrochemical corrosion process, forming a strain difference battery. Erosion can promote corrosion in desulfurization slurry, and grain boundary corrosion also accelerates material stripping.

4. CONCLUSIONS

In the present study, an experimental system was built to investigate the erosion−corrosion effects of desulfurization slurry on three stainless steel samples, including 304, 316L, and 2205. The influences of eroding velocity, slurry temperature, chloride content, and duration time were mainly emphasized, with elucidation on the characteristics of mass loss and micromorphology. The following conclusions were mainly obtained.

Stainless steel 2205 has the strongest erosion resistance to simulated desulfurization slurry, while type 304 shows serious corrosion. The erosion effect at the initial stage is predominant. The interaction between erosion and corrosion possibly decreases with an increase in the eroding velocity. The corrosion rate of the primary stainless steel is greatly temperature-dependent. The erosion−corrosion rate is weak at low temperatures, while the increase in the slurry temperature exacerbates the erosion−corrosion rate. The influence of temperature on the corrosion resistance of 304 is much greater than that of 2205. The rise of slurry temperature strengthens the difference between the 304 sample and the other two materials but weakens the diversity between 316L and 2205 samples. The high concentration of chloride ions yields a strong adverse effect on stainless steel serving in corrosive media, and proper control of chloride content in the slurry could extend the life of the equipment. Type 2205 has good chlorine corrosion resistance due to the characteristics of duplex stainless steel. With the gradual increase of corrosion time, the weight loss rate of stainless steel in the desulfurization slurry declines, and the changing trend of metal mass gradually slows down. Erosion−corrosion is a type of damage associated with the synergistic effects of mechanical, chemical, or/and electrochemical processes.

AUTHOR INFORMATION

Corresponding Author

Chang'an Wang − *State Key Laboratory of Multiphase Flow in Power Engineering, School of Energy and Power Engineering, Xi'an Jiaotong University, Xi'an 710049, China;* orcid.org/0000-0002-1730-740X; Email: changanwang@mail.xjtu.edu.cn

Authors

Gaofeng Fan − *State Key Laboratory of Multiphase Flow in Power Engineering, School of Energy and Power Engineering, Xi'an Jiaotong University, Xi'an 710049, China; Henan*

https://doi.org/10.1021/acsomega.3c09065
ACS Omega 2024, 9, 7132−7142

Hanzhiyue New Material Co., Ltd., Zhengzhou 450000, China

Jinming Zhang − *State Key Laboratory of Multiphase Flow in Power Engineering, School of Energy and Power Engineering, Xi'an Jiaotong University, Xi'an 710049, China*

Tianlin Yuan − *State Key Laboratory of Multiphase Flow in Power Engineering, School of Energy and Power Engineering, Xi'an Jiaotong University, Xi'an 710049, China*

Yujie Hou − *State Key Laboratory of Multiphase Flow in Power Engineering, School of Energy and Power Engineering, Xi'an Jiaotong University, Xi'an 710049, China*

Xinyue Gao − *State Key Laboratory of Multiphase Flow in Power Engineering, School of Energy and Power Engineering, Xi'an Jiaotong University, Xi'an 710049, China*

Jie Xu − *Henan Hanzhiyue New Material Co., Ltd., Zhengzhou 450000, China*

Defu Che − *State Key Laboratory of Multiphase Flow in Power Engineering, School of Energy and Power Engineering, Xi'an Jiaotong University, Xi'an 710049, China;* orcid.org/0000-0003-1881-4136

Complete contact information is available at: https://pubs.acs.org/10.1021/acsomega.3c09065

Notes

The authors declare no competing financial interest.

■ ACKNOWLEDGMENTS

The financial support from the National Natural Science Foundation of China (52176129) and the Natural Science Basic Research Plan in Shaanxi Province of China (2019JM-067) is greatly acknowledged.

■ REFERENCES

(1) Chen, H.; Wang, Y. H.; An, L. M.; Xu, G.; Zhu, X.; Liu, W. Y.; Lei, J. Performance Evaluation of a Novel Design for the Waste Heat Recovery of a Cement Plant Incorporating a Coal-Fired Power Plant. *Energy* **2022**, *246*, No. 123420, DOI: 10.1016/j.energy.2022.123420.

(2) Li, Y. Y.; Chen, X.; Jiang, S.; Lu, G. Thermodynamics of Cascaded Waste Heat Utilization from Flue Gas and Circulating Cooling Water. *J. Therm. Sci.* **2023**, *32* (5), 1737−1749.

(3) Zhang, L.; Zhao, C. X.; Sun, E. H.; Ji, H. F.; Meng, W. Z.; Zhang, Q.; An, G. Y. Energy, Exergy and Economic (3e) Study on Waste Heat Utilization of Gas Turbine by Improved Recompression Cycle and Partial Cooling Cycle. *Energy Sources, Part A* **2023**, *45* (2), 4127−4145.

(4) Teng, D.; Jia, X.; Yang, W.; An, L.; Shen, G.; Zhang, H. Experimental Investigation into Flue Gas Water and Waste Heat Recovery Using a Purge Gas Ceramic Membrane Condenser. *ACS Omega* **2022**, *7* (6), 4956−4969.

(5) Liu, Y.; Liu, S.; Duan, C. In *A Case Analysis and Treatment Measures of High Moisture Content in Wet Desulphurization Gypsum*, IOP Conference Series: Earth and Environmental Science; IOPScience, 2023.

(6) Kang, Q. H.; Yuan, Y. Diagnosis and Traceability Analysis of Slurry Foaming of Limestone-Gypsum Wet Flue-Gas Desulfurization (WFGD) System. *Water, Air, Soil Pollut.* **2023**, *234* (2), No. 108, DOI: 10.1007/s11270-023-06135-9.

(7) Yakah, N.; Noor, I. E.; Martin, A.; Simons, A.; Samavati, M. Wet Flue Gas Desulphurization (FGD) Wastewater Treatment Using Membrane Distillation. *Energies* **2022**, *15* (24), No. 9439, DOI: 10.3390/en15249439.

(8) Liang, Z. W.; Qi, T. Y.; Liu, H.; Wang, L. D.; Li, Q. W. Zero-Valent Bimetallic Catalyst/Absorbent for Simultaneous Facilitation of $Mgso_3$ Oxidation and Arsenic Uptake. *Sci. Total Environ.* **2022**, *844*, No. 157147, DOI: 10.1016/j.scitotenv.2022.157147.

(9) Shen, Z. G.; Guo, S. P.; Kang, W. Z.; Zeng, K.; Yin, M.; Tian, J. Y.; Lu, J. The Kinetics of Oxidation Inhibition of Magnesium Sulfite in the Wet Flue Gas Desulphurization Process. *Energy Sources, Part A* **2013**, *35* (20), 1883−1890.

(10) Chahartaghi, M.; Dahmardeh, N.; Hashemian, S. M.; Malek, R. Technical, Economic, and Environmental Analyses of Cchp Systems with Waste Incineration Power Plant as Prime Mover *Energy Sources, Part A* 2021 DOI: 10.1080/15567036.2021.1968074.

(11) Schütz, A.; Günthner, M.; Motz, G.; Greissl, O.; Glatzel, U. High Temperature (Salt Melt) Corrosion Tests with Ceramic-Coated Steel. *Mater. Chem. Phys.* **2015**, *159*, 10−18.

(12) Chung, R. J.; Tang, X.; Li, D. Y.; Hinckley, B.; Dolman, K. Microstructure Refinement of Hypereutectic High Cr Cast Irons Using Hard Carbide-Forming Elements for Improved Wear Resistance. *Wear* **2013**, *301* (1−2), 695−706.

(13) Krawczyk, B.; Cook, P.; Hobbs, J.; Engelberg, D. L. Corrosion Behavior of Cold Rolled Type 316l Stainless Steel in Hcl-Containing Environments. *Corrosion* **2017**, *73* (11), 1346−1358.

(14) Dong, C.; Luo, H.; Xiao, K.; Sun, T.; Liu, Q.; Li, X. Effect of Temperature and Cl-1 Concentration on Pitting of 2205 Duplex Stainless Steel. *J. Wuhan Univ. Technol., Mater. Sci. Ed.* **2011**, *26* (4), 641−647.

(15) Zhou, Y.; Engelberg, D. L. Fast Testing of Ambient Temperature Pitting Corrosion in Type 2205 Duplex Stainless Steel by Bipolar Electrochemistry Experiments. *Electrochem. Commun.* **2020**, *117*, No. 106779, DOI: 10.1016/j.elecom.2020.106779.

(16) Zhang, B.; Wang, J.; Liu, H.; Yan, Y.; Jiang, P.; Yan, F. Tribocorrosion Properties of Aisi 1045 and Aisi 2205 Steels in Seawater: Synergistic Interactions of Wear and Corrosion. *Friction* **2021**, *9* (5), 929−940.

(17) Chen, J.; Zhang, Q.; Li, Q.-A.; Fu, S.-L.; Wang, J.-Z. Corrosion and Tribocorrosion Behaviors of Aisi 316 Stainless Steel and Ti6al4v Alloys in Artificial Seawater. *Trans. Nonferrous Met. Soc. China* **2014**, *24* (4), 1022−1031.

(18) Tian, H. H.; Addie, G. R.; Visintainer, R. J. Erosion-Corrosion Performance of High-Cr Cast Iron Alloys in Flowing Liquid-Solid Slurries. *Wear* **2009**, *267* (11), 2039−2047.

(19) Parker, M. E.; Horton, D. J.; Wahl, K. J. Tribocorrosion Behavior of 2205 Duplex Stainless Steel in Sodium Chloride and Sodium Sulfate Environments. *Tribol. Lett.* **2022**, *70* (3), No. 70, DOI: 10.1007/s11249-022-01601-7.

(20) Renner, P.; Chen, Y.; Huang, Z.; Raut, A.; Liang, H. Tribocorrosion Influenced Pitting of a Duplex Stainless Steel. *Lubricants* **2021**, *9* (5), No. 52, DOI: 10.3390/lubricants9050052.

(21) Stack, M. M.; Abd El Badia, T. M. On the Construction of Erosion-Corrosion Maps for Wc/Co-Cr-Based Coatings in Aqueous Conditions. *Wear* **2006**, *261* (11−12), 1181−1190.

(22) Islam, M. A.; Farhat, Z. Erosion-Corrosion Mechanism and Comparison of Erosion-Corrosion Performance of Api Steels. *Wear* **2017**, *376-377*, 533−541.

(23) Aiming, F.; Jinming, J.; Ziyun, T. Failure Ananlysis of the Impeller of a Slurry Pump Subjected to Corrosive Wear. *Wear* **1995**, *181−183*, 876−882, DOI: 10.1016/0043-1648(95)90210-4.

(24) Dastgheib, S. A.; Mock, J.; Salih, H. H.; Patterson, C. Utilization of Water Utility Lime Sludge for Flue Gas Desulfurization in Coal-Fired Power Plants: Part Ill. Testing at a Higher Scale and Assessment of Selected Potential Operational Issues. *Energy Fuels* **2019**, *33* (11), 11536−11543.

(25) Smith, F.; Brownlie, F.; Hodgkiess, T.; Toumpis, A.; Pearson, A.; Galloway, A. M. Effect of Salinity on the Corrosive Wear Behaviour of Engineering Steels in Aqueous Solutions. *Wear* **2020**, *462−463*, No. 203515.

(26) Li, H.; Yang, X. Y.; Yin, X. Z.; Wang, X. W.; Tang, J. Q.; Gong, J. M. Effect of Chloride Impurity on Corrosion Kinetics of Stainless Steels in Molten Solar Salt for Csp Application: Experiments and Modeling. *Oxid. Met.* **2021**, *95* (3−4), 311−332, DOI: 10.1007/s11085-021-10025-y.

(27) Maher, M.; Iraola-Arregui, I.; Ben Youcef, H.; Rhouta, B.; Trabadelo, V. The Synergistic Effect of Wear-Corrosion in Stainless

Steels: A Review. *Mater. Today: Proc.* **2020**, *51*, 1975−1990, DOI: 10.1016/j.matpr.2021.05.010.
(28) Shahali, H.; Ghasemi, H. M.; Abedini, M. Contributions of Corrosion and Erosion in the Erosion-Corrosion of Sanicro28. *Mater. Chem. Phys.* **2019**, *233*, 366−377.
(29) Elemuren, R.; Evitts, R.; Oguocha, I.; Kennell, G.; Gerspacher, R.; Odeshi, A. Slurry Erosion-Corrosion of 90° Aisi 1018 Steel Elbow in Saturated Potash Brine Containing Abrasive Silica Particles. *Wear* **2018**, *410-411*, 149−155.
(30) Elemuren, R.; Evitts, R.; Oguocha, I. N. A.; Szpunar, J.; Kennell, G.; Gerspacher, R.; Tiamiyu, A. A.; Odeshi, A. G. Synergistic Erosion-Corrosion Behavior of Aisi 2205 Duplex Stainless Steel Elbows in Potash Brine-Sand Slurry and the Associated Microstructural Changes. *J. Mater. Eng. Perform.* **2020**, *29* (11), 7456−7467.
(31) Luo, J. H.; Yan, P.; Fan, Y. J.; Luo, S. J.; Long, Y. Investigation of Corrosion Behavior of 2205 Duplex Stainless Steel Coiled Tubing in Complex Operation Environments of Oil and Gas Wells. *Eng. Failure Anal.* **2023**, *151*, No. 107355.
(32) Labiapari, W. S.; Ardila, M. A. N.; Binder, C.; Costa, H. L.; De Mello, J. D. B. Mechanical Effects on the Corrosion Resistance of Ferritic Stainless Steels During Microabrasion-Corrosion. *Wear* **2019**, *426−427*, 1474−1481, DOI: 10.1016/j.wear.2018.12.057.
(33) Jones, M.; Llewellyn, R. J. Erosion-Corrosion Assessment of Materials for Use in the Resources Industry. *Wear* **2009**, *267* (11), 2003−2009.
(34) Ahmed, S.; Thakare, O. P.; Shrivastava, R.; Sharma, S.; Sapate, S. G. A Review on Slurry Abrasion of Hard Faced Steels. *Mater. Today: Proc.* **2017**, *5*, 3524−3532, DOI: 10.1016/j.matpr.2017.11.600.
(35) Li, P.; Zhao, Y. J.; Wang, L. B. Research on Erosion-Corrosion Rate of 304 Stainless Steel in Acidic Slurry Via Experimental Design Method. *Materials* **2019**, *12* (14), No. 2330, DOI: 10.3390/ma12142330.
(36) Li, L. L.; Wang, Z. B.; Zheng, Y. G. Interaction between Pitting Corrosion and Critical Flow Velocity for Erosion-Corrosion of 304 Stainless Steel under Jet Slurry Impingement. *Corros. Sci.* **2019**, *158*, No. 108084.
(37) Xiao, H. P.; Liu, S. H.; Wang, D. G.; Chen, Y. Abrasion-Corrosion Behaviors of Steel-Steel Contact in Seawater Containing Abrasive Particles. *Tribiol. Trans.* **2018**, *61* (1), 12−18.
(38) Chung, R. J.; Jiang, J.; Pang, C.; Yu, B.; Eadie, R.; Li, D. Y. Erosion-Corrosion Behaviour of Steels Used in Slurry Pipelines. *Wear* **2021**, *477*, No. 203771.
(39) Yu, R. Q.; He, J. J.; Li, W.; Ren, Y. J.; Yang, W. Erosive Wear of Cr30A High Chromium Cast lron in a Simulated Circulating Pump Operation Condition with Slurry Related to Wet Desulfuration Process in Thermal Power Plant. *J. Chin. Soc. Corros. Prot.* **2019**, *39* (04), 353−358.
(40) Raj, P. N.; Raha, B.; Sekar, K.; Joseph, M. A. Effect of Manganese on Synergistic Erosion-Corrosion Characteristics of A890 7a Hyper Duplex Stainless Steels. *J. Mater. Eng. Perform.* **2022**, *31* (1), 11−23.
(41) Lv, J.; Guo, W.; Liang, T. The Effect of Pre-Deformation on Corrosion Resistance of the Passive Film Formed on 2205 Duplex Stainless Steel. *J. Alloys Compd.* **2016**, *686*, 176−183.
(42) Ben Saada, F.; Elleuch, K.; Ponthiaux, P. On the Tribocorrosion Responses of Two Stainless Steels. *Tribiol. Trans.* **2018**, *61* (1), 53−60.
(43) Gao, R.; Liu, E.; Zhang, Y.; Zhu, L.; Zeng, Z. Tribocorrosion Behavior of Saf 2205 Duplex Stainless Steel in Artificial Seawater. *J. Mater. Eng. Perform.* **2019**, *28* (1), 414−422.

https://doi.org/10.1021/acsomega.3c09065
ACS Omega 2024, 9, 7132−7142